DOI: 10.15480/882.9320

Eighth International Symposium on Marine Propulsors
smp'24, Berlin, Germany, March 2024

Visualizing cavitation inception in tip leakage flow of a ducted marine propeller*

Ayush Saraswat[1], Chintan Panigrahi[1], Joseph Katz[1]

[1]Department of Mechanical Engineering, Johns Hopkins University (JHU), Baltimore, MD, USA

ABSTRACT

This paper presents results from high-speed visualization of tip leakage cavitation in a two-bladed ducted marine propeller. The observations highlight the cavitation around the blade tip. Included are: (i) traveling bubble cavitation in the tip gap, (ii) cavitation in the tip leakage vortex (TLV) that rolls up on the blade suction side (SS), (iii) and cavitating secondary structures engulfed from the blade pressure side (PS) to the SS. The secondary vortex filaments originate either from the pressure side of the blade or in the case of low advance ratios, from remnants of the TLV generated by the previous blade. As these filaments cross the tip gap, they are typically oriented perpendicularly to the blade chord. While being entrained, they appear to be associated with kinks or meandering of the TLV trajectory in the aft part and downstream of the blade, eventually resulting in TLV breakup. In all cases, cavitation inception appears as intermittent local elongated events along the TLV, typically in the aft part of the passage, hence away from the blade surface. At the same advance ratio, upon reduction in pressure, first the entire TLV core becomes filled with cavitation, which then expands to secondary structures and causes earlier kinking of the TLV. With further reduction in pressure, traveling bubble cavitation develops in the tip gap, filling the region between the TLV and the blade SS with cavitation, resulting in fragmentation of the TLV and formation of large cavitating vortices oriented in multiple directions. At the same cavitation index, with decreasing advance ratio, the cavitation in the TLV core thickens and starts closer to the leading edge, the vortex migrates farther from the blade SS, and starts meandering and breaking up early, presumably under the growing influence of more intense secondary vortices. Hence, both the advance ratio and the extent of cavitation alters the TLV trajectory, shape, and breakup.

Keywords

Ducted propeller, cavitation, high-speed imaging, tip leakage vortex.

1 INTRODUCTION

Cavitation in marine propulsors is known to cause unsteady loading, noise, and erosion. Consequently, understanding the origin, causes, growth, and dependence on flow variables is of interest to the propulsor design community. Over hydrodynamic lifting surfaces, such as hydrofoils and rotating blades, cavitation inception often occurs in the tip vortex (Arndt 1981, Arndt et al 1991, Brewer 2002, Chesnakas and Jessup 2003) owing to the low pressure in its core. In the case of ducted hydrofoils and propellers, the onset of cavitation is associated with the tip leakage flow from the pressure side (PS) to the suction side (SS) of the blade, and its subsequent rollup to the tip leakage vortex (TLV) and associated secondary structures. While numerous studies have examined tip vortex cavitation around stationary lifting surfaces (Arndt et al 1991, Boulon et al 1999, Gopalan et al 2002, Murayama et al 2008, Russell et al 2023) or open propellers (Gindroz and Billet 1998, Hsiao and Chahine 2008, Barkmann et al 2011), less information is available about ducted propellers (Chesnakas and Jessup 2003, Oweis and Ceccio 2005). In these two examples, cavitation inception occurs downstream of the propeller, allowing observations on its occurrence and flow measurements in the relevant region. It is also suggested that the onset of cavitation involves interactions between the TLV and other vortices shedding from the blade which results in vortex stretching and reduction of pressure.

Performing detailed observation on cavitation, and flow and pressure measurements around an entire ducted propeller could be challenging because of the limited optical access to the tip gap region. To address this problem, we perform experiments in a facility where the refractive index of the fluid is matched with that of transparent casing and propeller blades (Miorini et al 2012, Tan et al 2015a). This approach allows us to perform unobstructed observations on the evolution of the TLV cavitation along the propeller blades and perform PIV measurements over the entire region, including the tip gap (Wu et al 2011, Chen et al 2017). The present paper focuses on describing the general characteristics of a cavitating TLV at varying advance ratios and inlet pressures. These observations will guide future flow and pressure measurements that will quantify the flow mechanisms involved. The experimental setup is presented in the next section, followed by the results, and conclusions.

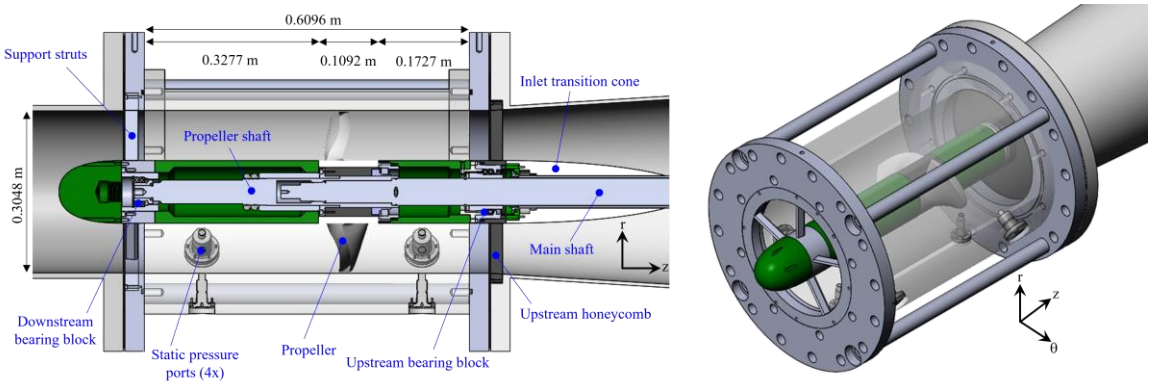

Figure 1: Transparent test section of the refractive index-matched two bladed ducted propeller. Left: A meridional cross-section showing the propeller support system; and Right: an isometric schematic.

2 METHODS AND FACILITY

The experiments are performed in the JHU refractive index matched test facility that has been described in multiple previous publications (Miorini et al 2012, Tan et al 2015a). The working fluid is an aqueous solution of sodium iodide that has a specific gravity of 1.832, and kinematic viscosity, $\nu=1.1\times10^{-6}$ m^2/s. The salt concentration is adjusted to match its refractive index with that of the acrylic blades and casing, providing unobstructed access for optical measurements. The propeller hub is made of black-anodized aluminum. The propeller shaft is connected to a 60 HP variable speed motor, and is equipped with a torque meter. To control the flow rate and pressure drop, the return line of the test loop has an additional 20 HP axial secondary propeller and a variable resistance valve consisting of perforated disks of varying blockage. The mean pressure is controlled by a vacuum pump and a source of compressed nitrogen, both of which are connected to a partially filled tank located above the test loop. Traversing a pitot tube in the return line in four planes inclined circumferentially by 45° to obtain the velocity profile and integrating it provides the flow rate. Differential pressure transducers are used for measuring the dynamic pressure of the pitot tube, the pressure upstream of the propeller (P_{in}), and if needed, the propeller pressure rise.

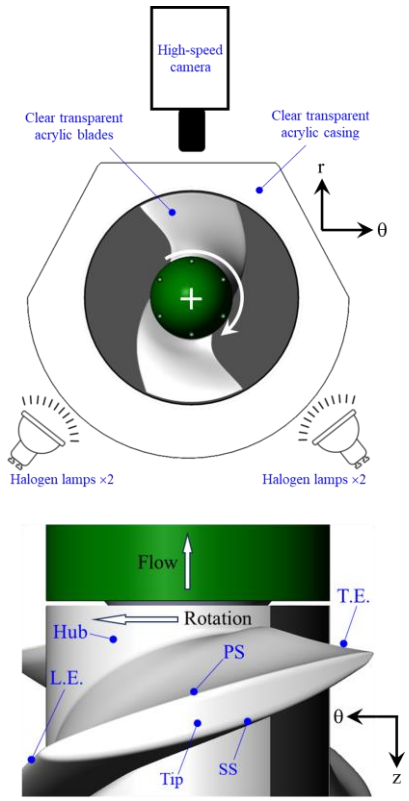

Figure 2: Experimental setup for high-speed cavitation visualization. Top: upstream looking view. Bottom: down looking view.

The high-speed imaging is performed on an acrylic, two-bladed, ducted, 1:3 replica, of model 5757 propeller (Figure 1) designed by the Naval Surface Warfare Center, Carderock Division (NSWCCD). The nominal inner casing diameter is 0.3048 m, and the nominal tip gap is 2.11 mm. The directly measured average tip gap is 1.96 mm, with standard deviation along the blade chord of both blades of 0.025 mm. The ball bearings upstream of the rotor are supported by a uniform stainless-steel honeycomb having a 3mm cell size to ensure a circumferentially uniform inflow. Downstream of the rotor, the shaft is supported through bearings by five streamlined struts. The experimental setup for observing the cavitation is shown in Figure 2. The 1024×976 pixel (1 MP) images are recorded at 25000 frames per second using a Phantom v2640 camera operating in the high-speed binning mode. The camera is equipped with a 60mm macrolens and the resulting field of view is 94.73×82.15 mm^2. Four continuous halogen lamps illuminate the tip region from below the test section. The cavitation inception tests are performed by recording images at 1000 fps while synchronizing the pressure transducer with the camera.

For all the results presented in this paper, the propeller speed is kept fixed at 572 RPM, and the flow rate, hence the advance ratio ($J=V/nD$, V being the inlet flow velocity, n being the speed in RPS, D being the nominal propeller tip diameter), is varied by changing the speed of the secondary propeller. The Reynolds number based on

the blade tip speed and chord length at 70% radius is 1.23×10^6. In all the cavitation images, the propeller rotates from right to left and the flow direction is from bottom to up. For calculating of the cavitation number, $\sigma=(p_{in}-p_v)/0.5\rho V^2$, the vapor pressure of the fluid (P_v) is taken as 1.2 kPa for the present temperature range, 21-23°C (Patil et al 1991, Tan et al 2015b).

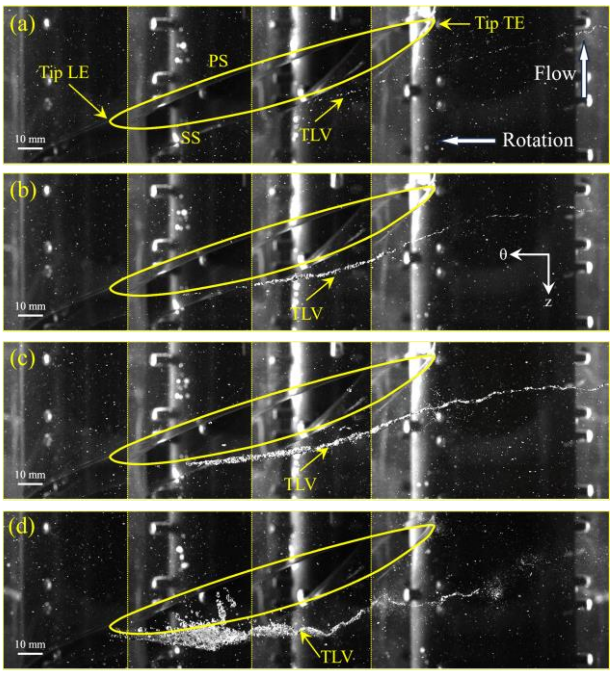

Figure 3: Tip leakage cavitation for inlet pressure of 59.3 kPa: (a) J=0.72, (b) J=0.68 (c) J=0.62, (d) J=0.56.

3 RESULTS

3.1 Effects of Advance Ratio (J)

Figure 3 shows examples of tip leakage cavitation at fixed inlet pressure of 59.3 kPa for four different advance ratios of J=0.72, 0.68, 0.62, and 0.56. The corresponding cavitation numbers, σ, are 14.90, 16.69, 20.08, and 24.62 respectively. Since the entire blade chord cannot be covered by a single field of view, we stack together multiple phase-lagged images from the same series that are delayed by a maximum time of 18 *ms*. The edges of individual frames are highlighted with dashed yellow lines. While one can observe, as expected, some variations in the cavitation topology from one blade pass to the next due to the unsteady nature of the flow and cavitation, its basic characteristics remain essentially unchanged. Consequently, in most cases, the stacking does not create a discontinuity. In all cases, the earliest signs of cavitation appear in the tip leakage vortex (TLV) developing along the suction side (SS) of the blade. With decreasing advance ratio, the cavitating TLV core thickens, starts closer to the leading edge (LE), and migrates axially farther from the blade SS. To clearly show these observations, the variation in mean TLV size and trajectory with advance ratio obtained over 20 blade passes is shown in Figure 4. These changes could be

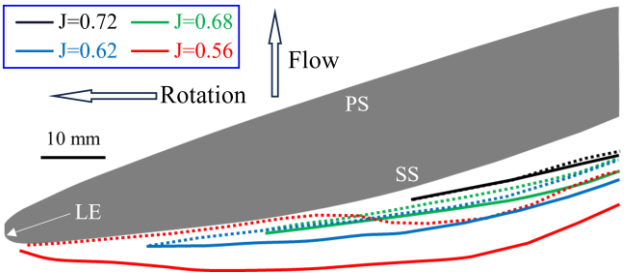

Figure 4: Mean cavitating TLV size and trajectory in the front part of the blade tip. Averaging performed over 20 blade passes. Solid color lines denote the upstream edge of the TLV cavitation and dashed color lines denote the downstream edge.

attributed to increasing blade loading with decreasing flow rate, which increases the leakage flow and vortex strength, and an upstream shift in the location of peak blade loading, which is expected to impact the location of TLV roll up (Li et al 2019).

The early TLV traces appear to be smooth, but then the TLV starts to meander and form kinks. With decreasing J, the point where the vortex starts meandering moves closer to the LE. This phenomenon is most likely associated with interaction with secondary structures that are engulfed from the PS to the SS of the blade, across the tip gap (Chen et al 2017). Clear indication of such entrainment and interaction is discussed further in subsection 3.3. Finally, at J=0.56 (Figure 3d), the distinct cavitating TLV disappears beyond the TE, and is replaced by a swirling bubble cloud. The same phenomenon occurs at higher J, but circumferentially farther from the blade, beyond the present field of view. We have seen a similar trend in a series of axial turbomachines (Miorini et al 2012, Tan et al 2015a, Li et al 2019), and have attributed it to vortex breakdown.

3.2 Effect of Cavitation Index(σ)

Figure 5 shows how the pressure affects the appearance of cavitation, all at J=0.56. At σ=38.2 (Figure 5a) the TLV cavitation is still discontinuous, but appears in multiple spots along the vortex core. Upon lowering σ to 29 (Figure 5b), the cavitation expands to the entire TLV, becoming continuous. With further reduction in σ to 24.6 (Figure 5c), traveling bubble cavitation appears in the tip gap along with cavitating secondary structures that extend from the PS to the SS almost perpendicularly to the blade chord. As the cavitation originated from the tip gap is entrained into the TLV, it also fills the space between the SS tip and the vortex core. While the core can be seen further along the blade, kinks and discontinuities appear in its trajectory and shape. At even lower pressures, σ<=21.2 (Figures 5d-5f), the traveling bubble cavitation expands to the entire blade tip, and the generated bubbles fill the entire region between the blade SS and the TLV. Eventually, the TLV core disappears and is replaced by a series of large cavitating vortices aligned in different directions. At these low pressures, attached cavitation also appears along the blade's SS surface. Note that beyond

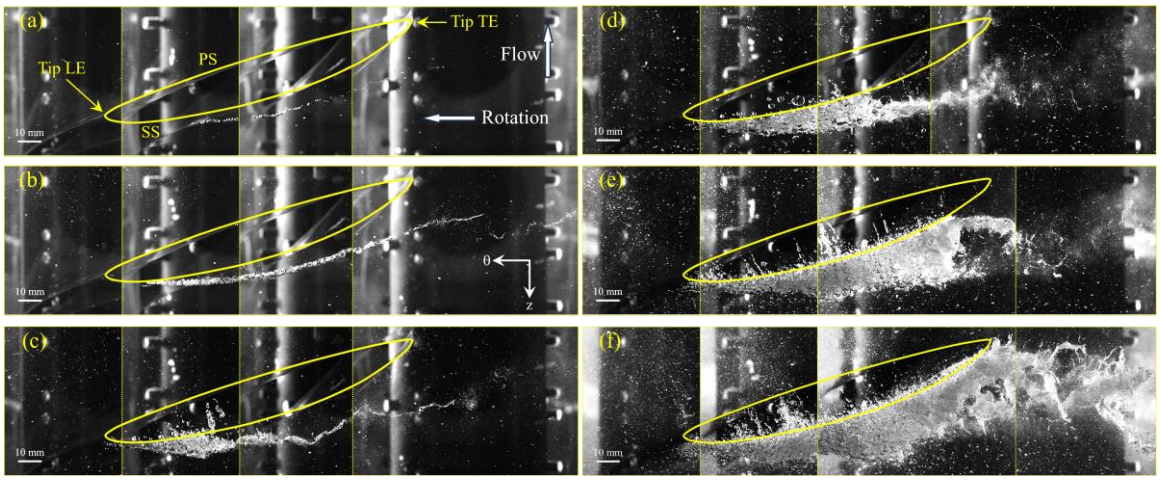

Figure 5: Cavitation at J=0.56 for inlet pressure and cavitation number: (a) 91 kPa, σ=38.2 (b) 69.6 kPa, σ=29 (c) 59.3 kPa, σ=24.6 (d) 51 kPa, σ=21.2 (e) 38.6 kPa, σ=15.8 (f) 32.4 kPa, σ=13.3

the early phase of cavitation, i.e., σ<=21.2 in Figure 5, the vortex location changes with decreasing pressure.

3.3 Secondary Vortical Structures

The term 'secondary vortical structures' refers to vortices present in the tip region of the propeller other than the TLV. Based on prior studies, these structures originate from three possible sources: (i) rollup of the PS vorticity into vortices that are aligned perpendicularly to the blade chord in varying locations along the blade, which are then entrained across the tip gap with the leakage flow (Wu et al 2011, Miorini et al 2012), (ii) interaction of the leakage flow with the main passage flow radially inward of the TLV on the blade SS (Chen et al 2017), and (iii) remnants of the TLV of a previous blade following its breakup, especially at low advance ratio when these remnants pass near the PS of the next blade (Hah 2017). Figure 6 is a sample time sequence (J=0.68, σ=13.7) highlighting cavitation in secondary structures, which are located radially outward of the TLV, and axially between the SS and the TLV. These vortices curl around the TLV, and appear to be located near the vortex kinks, suggesting that they play a role in causing the TLV discontinuity, a phenomena seen before in multiple studies (Chesnakas and Jessup 2003, Oweis and Ceccio 2005, Oweis et al 2006). Striking examples of secondary structures associated with blade to blade interactions are presented in Figure 7, this time at J=0.56 and σ=13.3. Here, the distinct TLV structure disappears, owing to vortex breakdown, and is replaced by a cloud containing multiple large vortices, some of them aligned perpendicularly to the blade. Part of these large structures extend to the leading edge of the next blade (Figure 7c) and others are entrained across the tip gap (Figure 7d). This example is an extreme case, where extensive cavitation simplifies the visualization. However, entrainment of remnants of a previous TLV across the tip gap is also observed for the low J cases at higher pressures, but are difficult to decipher in still images.

3.4 Cavitation Inception

Inception of cavitation in the tip region of propellers has

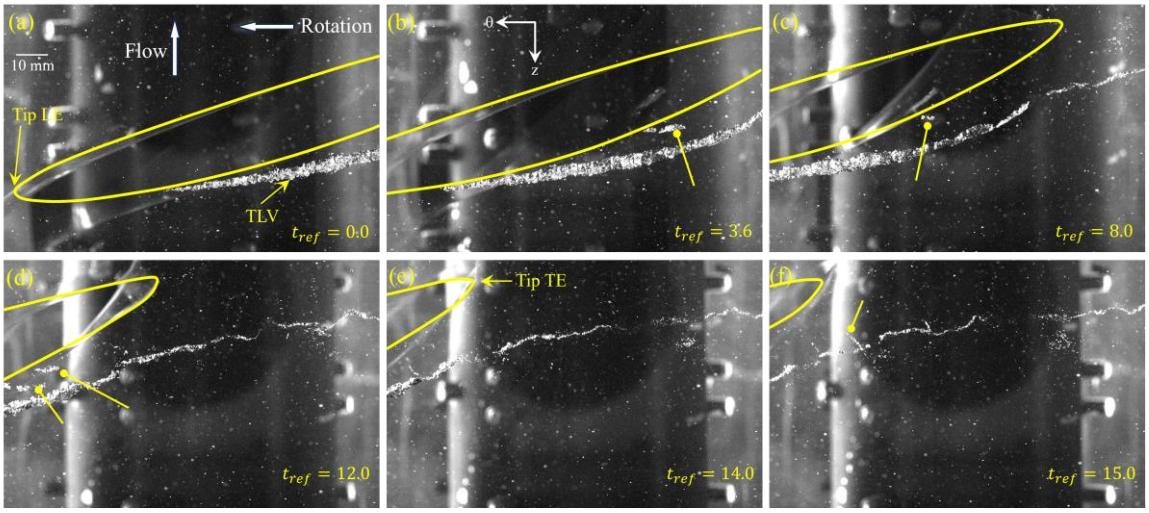

Figure 6: Cavitation in secondary vortical structures at J=0.68 for inlet pressure of 48.9 kPa and cavitation number of 13.7. Secondary structures are marked by arrows with circular head. Time is in milliseconds.

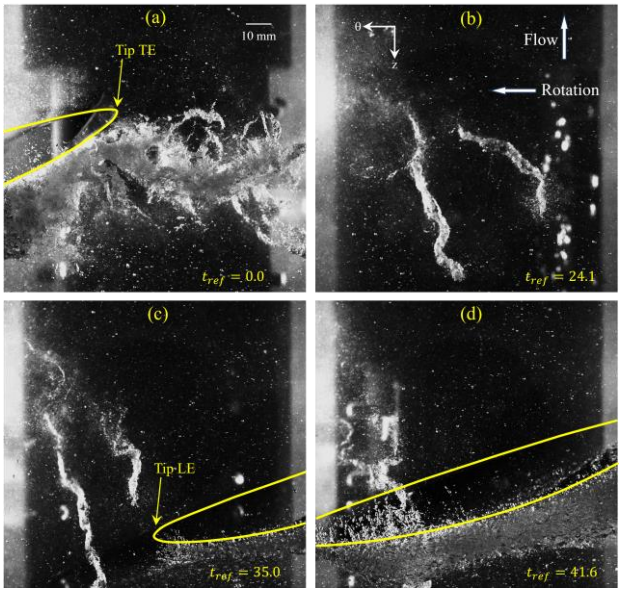

Figure 7: Cavitation in secondary vortical structures at J=0.56 for inlet pressure of 32.4 kPa and cavitation number of 13.3. Time is in milliseconds.

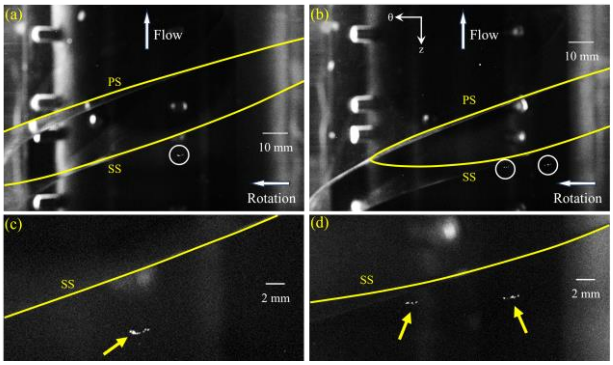

Figure 8: (a, b): Examples of cavitation inception events at J=0.56. (c, d): Zoomed-in view of (a) and (b) respectively.

been associated with the interaction of the TLV and secondary structures (Chesnakas and Jessup 2003, Oweis and Ceccio 2005). For instance, Chesnakas and Jessup (2003) show that inception occurs at the point where the TLV interacts with the so-called "trailing edge vortex", a secondary structure originating at the tip TE. In their case, this point is located on the SS, i.e., axially upstream of the TE, and circumferentially downstream of the blade ($\theta<\theta_{TE}$). Two images of the onset of cavitation near the present propeller tip at J=0.56 are presented in Figure 8, with the bottom row showing a magnified part of the top row. In both cases, the early cavities appear on the SS, in the mid-chord region, along what the previous two sections show is the TLV trajectory (see Figures 3, 4, and 5). These elongated events appear intermittently at different sites, and in one of the cases (Figure 8b and 8d), two cavities appear in different locations essentially at the same time. This trend is consistent with the appearance of multiple secondary structures at different locations along the blade tip, as discussed in the previous section. Inception tests, which include statistics of both the locations and the cavitation inception indices for the present range of advance ratios are presently in progress.

4 SAMPLE STEREO-PIV RESULTS

In this section, we show sample results from the ongoing stereo-PIV measurements aimed at elucidating the flow structure in the tip region of the propeller. The data acquisition is being carried out in a meridional (r-z) plane at multiple blade orientations using a pair of 29MP Imperx B6640 CCD cameras. The achieved vector spacing, using a final interrogation window size of 32×32 pixels, and 50% overlap, is 0.17 mm over a field of view of 45.1 × 18.6 mm^2. Figure 9 shows two sample distributions of axial and circumferential velocity components along with the circumferential vorticity ensemble-averaged over 500 instantaneous realizations for J=0.68 and J=0.56. All samples also show the in-plane velocity vectors, i.e. the axial and radial velocity components. Here, the axial velocity is normalized by the area-averaged axial velocity (V_z), i.e. the flow rate divided by the through-flow area. The circumferential velocity and vorticity are normalized by the blade tip speed (U_T) and the blade angular velocity (Ω, in rad/s), respectively. In these plots, the z-axis is normalized by the axial chord (c_a) and the radial coordinates are expressed as $r^*=(r-r_h)/(r_c-r_h)$, where the subscripts h and c refer to the blade hub and casing, respectively. However, the scales are adjusted to keep the aspect ratio of the plots consistent with the physical scales. In both examples, the light sheet dissects the blade at s/c=0.875, where c is the blade tip chord, and s is a chordwise coordinate, such that s/c=0 refers to the blade tip LE and s/c=1 to the blade tip TE. For clarity, the vectors are diluted by 4:1 in the axial direction.

The prominent flow features include a leakage flow in the tip gap from the PS to the SS of the blade, which rolls up into a TLV on the SS. With decreasing J, the leakage flow becomes stronger, hence it jets out further upstream. The TLV center is identified by a peak in positive circumferential vorticity whose location extends further upstream with decreasing J, consistent with the trends depicted in the cavitation images. In both examples, the locations of the TLV centers are consistent with those visualized at low levels of cavitation (figure 5b and 6b). A positive vorticity shear layer extends from the TLV center to the SS tip. This shear layer defines the boundary between the backward leakage flow and the forward passage flow under it. Flow induced by the TLV also causes endwall separation and entrains the casing boundary layer away from the wall, creating a negative circumferential vorticity layer that surrounds the upstream end of the TLV. These flow features have been seen before in other axial turbomachines, such as waterjet pumps and aviation compressors (Miorini et al 2012, Li et al 2019). At high J (J=0.68), the circumferential velocity in the tip gap is positive, i.e. opposite to the direction of blade motion, but it changes to a negative direction at J=0.56. This trend has also been seen before in aviation

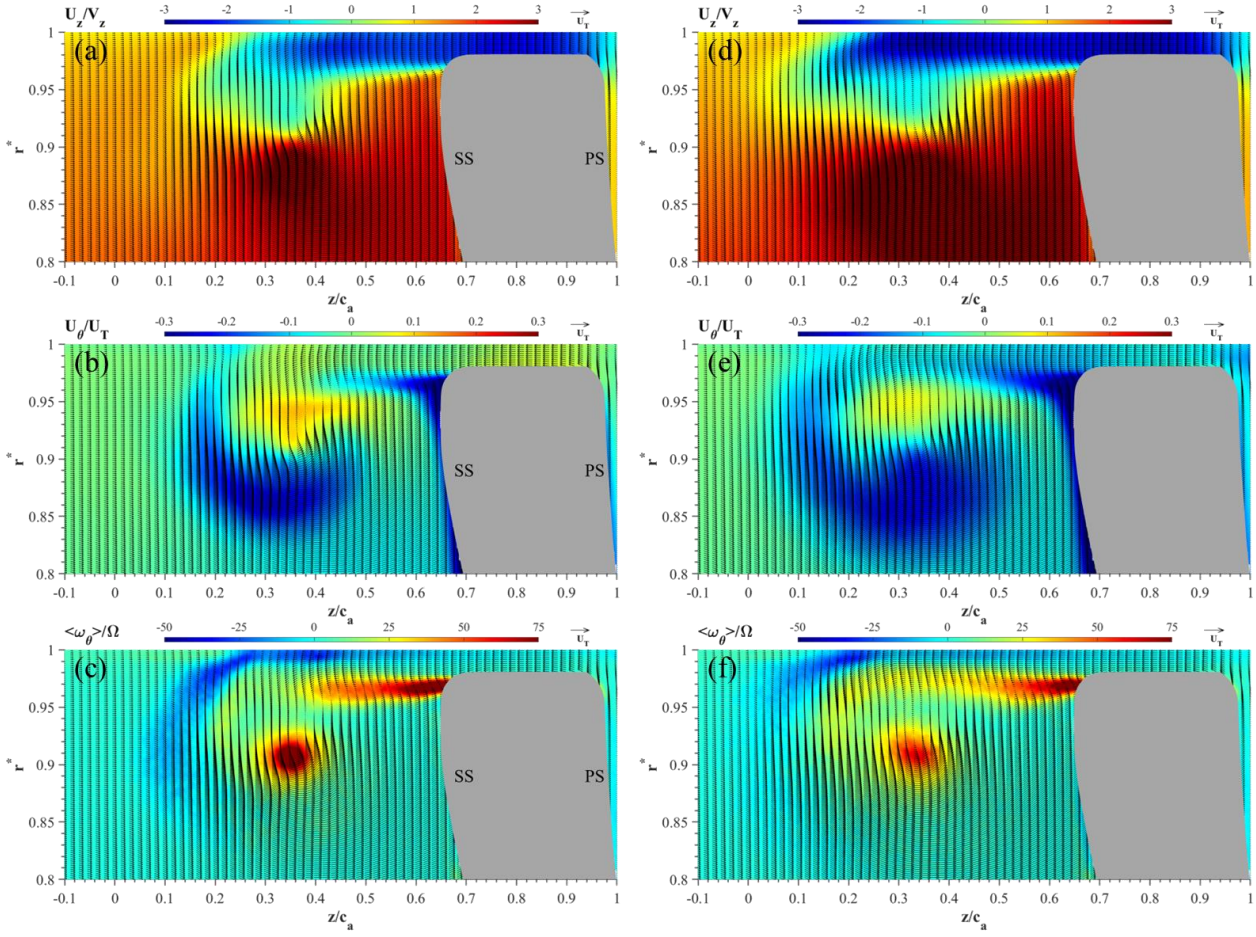

Figure 9: Ensemble-averaged velocity and vorticity in the tip region at s/c=0.875. Left, J=0.68. Right, J=0.56. (a, e): Axial velocity, U_z/V_z. (b, d) Circumferential velocity, U_θ/U_T. (c, f) Circumferential vorticity, $\langle\omega_\theta\rangle/\Omega$.

compressors (Li et al 2019). Another consistent trend is the positive circumferential velocity above the TLV center and negative below it, implying that the TLV center is located in a region of radial gradients in U_θ.

5 CONCLUSIONS

High-speed imaging of cavitation in the tip region of a ducted marine propeller has been performed in a refractive index-matched facility. The observations characterize the variations in a cavitating TLV at varying cavitation indices and advance ratios. With decreasing advance ratio, but at the same pressure, the diameter of the cavitating core increases, cavitation appears and formation of TLV kinks occurs closer to the LE. The latter is attributed to interaction with secondary structures that appear at several locations along the blade tip and originate from three sources. Included are vortices formed due to (i) rollup of PS vorticity, that are entrained through the tip gap, (ii) interaction of leakage flow and main passage flow, (iii) remnants of the TLV of the previous blade, especially at low advance ratios.

At the same advance ratio, with decreasing cavitation number, the cavitation expands initially along the TLV, eventually filling its entire core, from rollup near the LE to the breakup point, typically circumferentially beyond the trailing edge. The TLV trajectory is also modified and becomes unsteady. Upon further reduction in pressure, cavitation occurs also in secondary structures, along with increasing traveling bubble cavitation in the tip gap. The resulting bubbles fill the gap between the blade SS and the TLV. Finally, the traveling bubble cavitation appears to disrupt the TLV structure, and its core is replaced by multiple cavitating vortices oriented in different directions. At low advance ratios, part of these structures either extend upstream of the next blade or are entrained across the tip gap and interact with the next TLV.

These observations provide important insights on the evolution of cavitation in the tip region and provide guidance in selecting sites for upcoming 2D and 3D particle image velocimetry experiments. These experiments are aimed at elucidating the evolution of the TLV structure and its interaction with the leakage flows.

ACKNOWLEDGEMENT

The work is supported by the Office of Naval Research (ONR) through grant number N00014-21-1-2833. The authors thank Dr. Thad Michael from Naval Surface Warfare Center Carderock Division (NSWCCD) for designing and providing propeller blade geometry. The authors express their gratitude to the late Dr. Yury Ronzhes who led the designing and fabrication efforts of the experimental rig and the turbomachine facility at the Johns Hopkins University (JHU). The experiments are part of the tip gap flow (TGF) project, which is a

collaboration between NSWCCD, JHU, University of Michigan, and Australian Maritime College (AMC) of University of Tasmania (UTAS).

REFERENCES

Arndt, R. E. (1981). 'Cavitation in fluid machinery and hydraulic structures.' Annual Review of Fluid Mechanics, 13(1).

Arndt, R., Arakeri, V., & Higuchi, H. (1991). 'Some observations of tip-vortex cavitation'. Journal of Fluid Mechanics, 229.

Barkmann, U., Heinke, H. J., & Lübke, L. (2011). 'Potsdam propeller test case (PPTC)'. Proceeding of the Second International Symposium on Marine Propulsors-smp'11.

Boulon, O., Callenaere, M., Franc, J. P., & Michel, J. M. (1999). 'An experimental insight into the effect of confinement on tip vortex cavitation of an elliptical hydrofoil.' Journal of Fluid Mechanics, 390.

Brewer, W. H. (2002). 'On simulating tip-leakage vortex flow to study the nature of cavitation inception.' Mississippi State University.

Chen, H., Li, Y., Tan, D., and Katz, J. (2017). 'Visualizations of Flow Structures in the Rotor Passage of an Axial Compressor at the Onset of Stall.' ASME. Journal of Turbomachinery, 139(4).

Chesnakas, C. J., & Jessup, S. D. (2003). 'Tip-vortex induced cavitation on a ducted propulsor'. Fluids Engineering Division Summer Meeting, Vol. 36967.

Gindroz, B., and Billet, M. L. (1998). 'Influence of the Nuclei on the Cavitation Inception for Different Types of Cavitation on Ship Propellers.' ASME. Journal of Fluids Engineering, 120(1).

Gopalan, S., Katz, J., & Liu, H. L. (2002). 'Effect of gap size on tip leakage cavitation inception, associated noise and flow structure'. Journal of Fluids Engineering, 124(4).

Hah, C. (2017). 'Effects of Double-Leakage Tip Clearance Flow on the Performance of a Compressor Stage With a Large Rotor Tip Gap.' ASME. Journal of Turbomachinery, 139(6).

Hsiao, C. T., & Chahine, G. L. (2008). 'Scaling of tip vortex cavitation inception for a marine open propeller.' In 27th symposium on naval hydrodynamics.

Li, Y., Chen, H., Tan, D., and Katz, J. (2019). 'On the Effects of Tip Clearance and Operating Condition on the Flow Structures Within an Axial Turbomachine Rotor Passage.' ASME. Journal of Turbomachinery, 141(11).

Miorini, R. L., Wu, H., and Katz, J. (2012). "The Internal Structure of the Tip Leakage Vortex Within the Rotor of an Axial Waterjet Pump." ASME. Journal of Turbomachinery, 134(3)

Murayama, M., Yoshida, Y., and Tsujimoto, Y. (2006). 'Unsteady Tip Leakage Vortex Cavitation Originating From the Tip Clearance of an Oscillating Hydrofoil.' ASME. Journal of Fluids Engineering, 128(3).

Oweis, G. F., & Ceccio, S. L. (2005). 'Instantaneous and time-averaged flow fields of multiple vortices in the tip region of a ducted propulsor'. Experiments in fluids, 38.

Oweis, G. F., Fry, D., Chesnakas, C. J., Jessup, S. D., and Ceccio, S. L. (2006). 'Development of a Tip-Leakage Flow—Part 1: The Flow Over a Range of Reynolds Numbers.' ASME Journal of Fluids Engineering, 128(4).

Patil, K. R., Tripathi, A. D., Pathak, G., & Katti, S. S. (1991). 'Thermodynamic properties of aqueous electrolyte solutions. 2. Vapor pressure of aqueous solutions of sodium bromide, sodium iodide, potassium chloride, potassium bromide, potassium iodide, rubidium chloride, cesium chloride, cesium bromide, cesium iodide, magnesium chloride, calcium chloride, calcium bromide, calcium iodide, strontium chloride, strontium bromide, strontium iodide, barium chloride, and barium bromide.' Journal of chemical and engineering data, 36(2).

Russell, P. S., Barbaca, L., Venning, J. A., Pearce, B. W., & Brandner, P. A. (2023). 'Influence of nucleation on cavitation inception in tip leakage flows'. Physics of Fluids, 35(1).

Tan, D., Li, Y., Wilkes, I., Miorini, R. L., and Katz, J. (2015a). 'Visualization and Time-Resolved Particle Image Velocimetry Measurements of the Flow in the Tip Region of a Subsonic Compressor Rotor.' ASME. Journal of Turbomachinery, 137(4).

Tan, D., Li, Y., Wilkes, I., Vagnoni, E., Miorini, R. L., and Katz, J. (2015b). 'Experimental Investigation of the Role of Large Scale Cavitating Vortical Structures in Performance Breakdown of an Axial Waterjet Pump.' ASME. Journal of Fluids Engineering, 137(11).

Wu, H., Tan, D., Miorini, R. L., & Katz, J. (2011). 'Three-dimensional flow structures and associated turbulence in the tip region of a waterjet pump rotor blade.' Experiments in fluids, 51.